Class-E current-driven center-tapped low dv/dt rectifierIAS '95. Conference Record of the 1995 IEEE Industry Applications Conference

CLASS–E CURRENT–DRIVEN CENTER–TAPPED LOW *dv/dt* RECTIFIER

M. Bartoli, A. Reatti, Member, IEEE
University of Florence,
Department of Electronic Engineering
Via di S. Marta, 3, 50139 Florence, Italy
Phone: (39)(55)4796–389 and Fax: (39)(55)494569
E – Mail: CIRCUITI@MAILSERVER.IDG.FI.CNR.IT

M. K. Kazimierczuk, Senior Member, IEEE
Wright State University,
Department of Electrical Engineering
Dayton, Ohio 45435
Phone: (513)873–5059 and Fax: (513)873–5009
E – Mail: MKAZIM@VALHALLA.CS.WRIGHT.EDU

Abstract — An analysis for a Class E current–driven center–tapped low *dv/dt* rectifier taking into account the transformer leakage inductances is given along with experimental verifications. The rectifier diodes turn on and off at low *dv/dt*. This results in low switching noise and low switching losses. Diode parasitic capacitances do not adversely affect the circuit operation. The absolute value of *di/dt* is limited at diode turn–off, reducing the reverse recovery current. The circuit is operated at a low output voltage ripple and, therefore, at a low power loss in the equivalent series resistance (ESR) of the filter capacitor. Experimental tests were performed for a rectifier circuit operated at an output power of P_O = 60 W, an minimum frequency of f = 500 kHz, and an output voltage of V_O = 3.3 V. The theoretical and the experimental results are in good agreement. Experimental measurements demonstrate that the rectifier is suitable for high–power density, high–frequency applications that requires low–output voltages and high–currents.

I. INTRODUCTION

The increasing demand for small–volume light–weight power supplies has necessitated the development of high–frequency high–efficiency power converter circuits. This can be achieved if switching losses are eliminated. In class E rectifiers [1]–[7], zero–voltage turn on of the diode is achieved. Moreover, the diodes turn on and off at low *dv/dt* resulting in low switching noise. Therefore, these rectifiers can be operated at high switching frequencies with a nearly constant efficiency over a wide load range [4]–[6]. In the class E current–driven center–tapped rectifier, the output voltage ripple is drastically reduced, the average current through each diode is one–half of the output current, and a lower volume transformer than in the class E full–wave rectifier [7] can be used. As a result, the class E current–driven center–tapped rectifier is suitable for high power–density applications at high–output currents, e.g., higher than 10 A and low–output voltages, e.g., 3.3 V or 5 V, which are the standard supply voltages of advanced VLSI circuits. Moreover, Class E rectifiers can be used in combination with class D and class E resonant inverters to build high–frequency dc–dc converters [8]–[21].

The purpose of this paper is to present an analysis and experimental results for a class E current–driven center–tapped low *dv/dt* rectifier. The rectifier was tested on a 60 W power supply operated at a line ac voltage ranging from 75 to 275 V_{rms}, an output current varying from 1.8 to 18 A, and an output voltage V_O = 3.3 V regulated over the entire line voltage and load current ranges. The nominal operating frequency of the converter circuit was f = 500 kHz. A maximum efficiency η = 80 % was achieved for the entire power supply at the maximum load and an ac input voltage V_{Irms} = 220 V.

II. CIRCUIT DESCRIPTION

A schematic circuit of the class E current–driven center–tapped low *dv/dt* rectifier and its model are shown in Figs. 1(a) and (b), respectively.

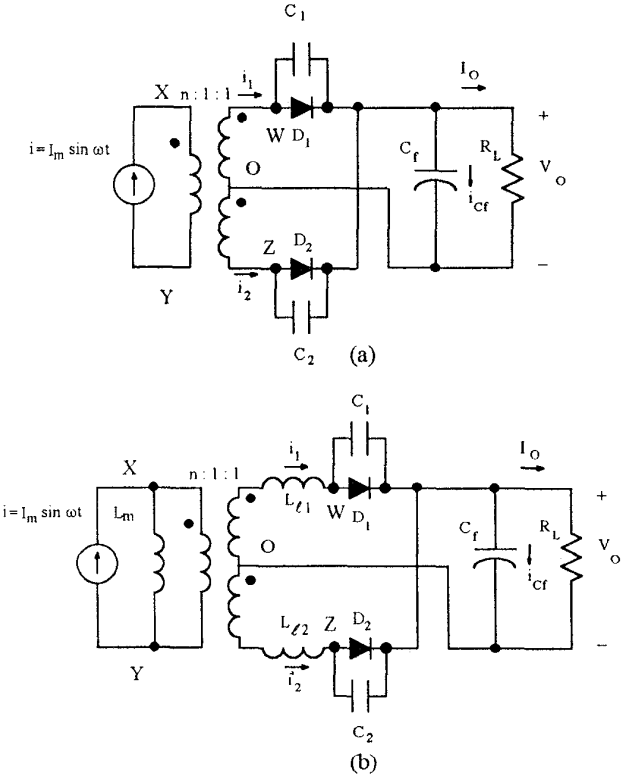

Fig. 1. Class E current–driven center–tapped low *dv/dt* rectifier. a) Schematic circuit. b) Model of the rectifier.

The rectifier consists of two diodes D_1 and D_2, two capacitors C_1 and C_2, a single–pole low–pass output filter C_f–R_L, and a center–tapped transformer with a turns ratio n. Resistor R_L is the dc load resistance. The diode parasitic capacitances are absorbed into capacitances C_1 and C_2 connected in parallel with the diodes. The entire leakage flux of the transformer has been taken into account by means of two

0-7803-3008-0/95 $4.00 © 1995 IEEE

leakage inductances $L_{\ell 1}$ and $L_{\ell 2}$ on the secondary side. L_m is the magnetizing inductance placed on the primary side of the transformer.

The transformer primary side is supplied by sinusoidal current source

$$i = I_m \sin \omega t \quad (1)$$

where I_m and $\omega = 2\pi f$ are the amplitude and the angular frequency of the current, respectively.

III. Principle Of Operation

The rectifier circuit can be operated at an on duty cycle of each diode D ranging from 0 to 1 and goes through four topological configurations during one switching period $T = 1/f$. These topological modes are defined by the diode states as given in Table I.

TABLE I.

RECTIFIER DIODE STATES.

	D_1	D_2
$0 < D \leq 0.5$		
$\phi \leq \omega t < \phi + 2\pi D$	ON	OFF
$\phi + 2\pi D \leq \omega t < \phi + \pi$	OFF	OFF
$\phi + \pi \leq \omega t < \phi + \pi + 2\pi D$	OFF	ON
$\phi + \pi + 2\pi D \leq \omega t < \phi + 2\pi$	OFF	OFF
$0.5 < D \leq 1$		
$\phi \leq \omega t < \phi + 2\pi D$	ON	OFF
$\phi + 2\pi D \leq \omega t < \phi + \pi$	ON	ON
$\phi + \pi \leq \omega t < \phi + \pi + 2\pi D$	OFF	ON
$\phi + \pi + 2\pi D \leq \omega t < \phi + 2\pi$	ON	ON

The current and voltage waveforms for the rectifier operated at $0 < D \leq 0.5$ and $0.5 < D \leq 1$ are shown in Figs. 2(a) and (b), respectively.

A. Operation for $0 < D \leq 0.5$

The first topological mode begins at $\omega t = \phi$, when voltage v_{D1} across diode D_1 reaches zero turning diode D_1 on. Actually, D_1 turns on when v_{D1} reaches the threshold voltage V_T, e.g., V_T = 0.4 V for Schottky diodes. During this time interval, current i_1 of the upper secondary winding flows through D_1. Diode D_2 is off and its voltage waveform is shaped by the shunt capacitor C_2, according to $i_{C2} = C_2\, dv_{C2}/dt$. The first mode ends at $\omega t = \phi + 2\pi D$, when current i_{D1} reaches zero, turning D_1 off.

During the second topological mode both D_1 and D_2 are OFF. Current i_1 flows through capacitor C_1, voltage $v_{D1} = v_{C1}$ is shaped according to $i_{C1} = C_1\, dv_{C1} / dt$. Since the capacitor current is zero at the beginning of the second topological mode, the derivative of v_{D1} is also zero at $\omega t = \phi + 2\pi D$. After diode D_1 turn-off, voltage v_{D1} slowly decreases because i_{C1} is negative. Since i_{C2} is positive, voltage v_{D2} increases and reaches the diode threshold voltage at $\omega t = \phi + \pi$, turning diode D_2 on. This ends the second mode.

The third topological mode begins at $\omega t = \phi + \pi$, when diode D_2 turns on and ends at $\omega t = \phi + \pi + 2\pi D$, when it turns off. During this time interval, the lower secondary winding current i_2 flows through diode D_2. The waveform of the voltage across diode D_1 and capacitor C_1 is still shaped by the current through C_1. Therefore, it decreases, reaches its minimum value V_{DM} when i_{C1} is zero, and then increases when i_{C1} is positive.

The fourth mode begins, when current i_{D2} reaches zero and diode D_2 turns off. As in the first topological mode, C_2 shapes the voltage waveform of D_2. Therefore, voltage v_{D2} slowly decreases from zero because i_{C2} is zero at $\omega t = \phi + \pi + 2\pi D$. The current through capacitor C_1 is positive and, therefore, voltage v_{D1} increases. Diode D_1 turns on at $\omega t = \phi + 2\pi$, when v_{D1} reaches the threshold voltage. This ends the fourth topological mode and the switching period.

B. Operation for $0.5 < D \leq 1$

The first and the third topological modes are identical for the first and the third topological modes of the rectifier operated at $0 < D \leq 0.5$. The second topological mode begins at $\omega t = \phi + \pi D$ when diode D_2 turns on and ends at $\omega t = \phi + 2\pi D$ when current i_1 decreases to zero turning off diode D_1. The fourth topological modes begins at $\omega t = \phi + \pi + 2\pi D$ when diode D_1 turn on and ends at $\omega t = \phi + 2\pi$ with the turn-off of diode D_2. During these two intervals both diodes are ON, terminals W and Z of the two secondary windings are shorted, and currents through these windings are $i_1 = -i_2$. The amplitudes of these current do not rise to dangerous values because the transformer primary side is driven by a current source.

III. Rectifier Circuit Analysis

The analysis of the Class E rectifier of Fig. 1(a) begins with the following assumptions.

1) The rectifier circuit is symmetrical. Therefore, $C_1 = C_2 = C_p$, and $L_{\ell 1} = L_{\ell 2} = L$.
2) The parasitic resistances of the core and the windings, and the transformer stray capacitances are neglected.
3) The diodes are ideal and identical, i.e., they have zero threshold voltage, zero on-resistance, infinite off-resistance, and zero minority carrier charge lifetime in the case of the *pn* junction diode.
4) Filter capacitor C_f is large enough to neglect the output voltage ripple. For this reason, the parallel combination of C_f and R_L can be replaced by a dc voltage source.
5) The sinusoidal current source driving the primary side of the rectifier transformer is ideal.
6) The transformer has a turns ratio of n for each secondary. Moreover, the winding and core resistances and the stray capacitance of the transformer are ignored. The magnetizing inductance L_m is assumed to be large enough to carry only a dc current. Therefore, it can be considered as an open circuit for the ac component of the current.

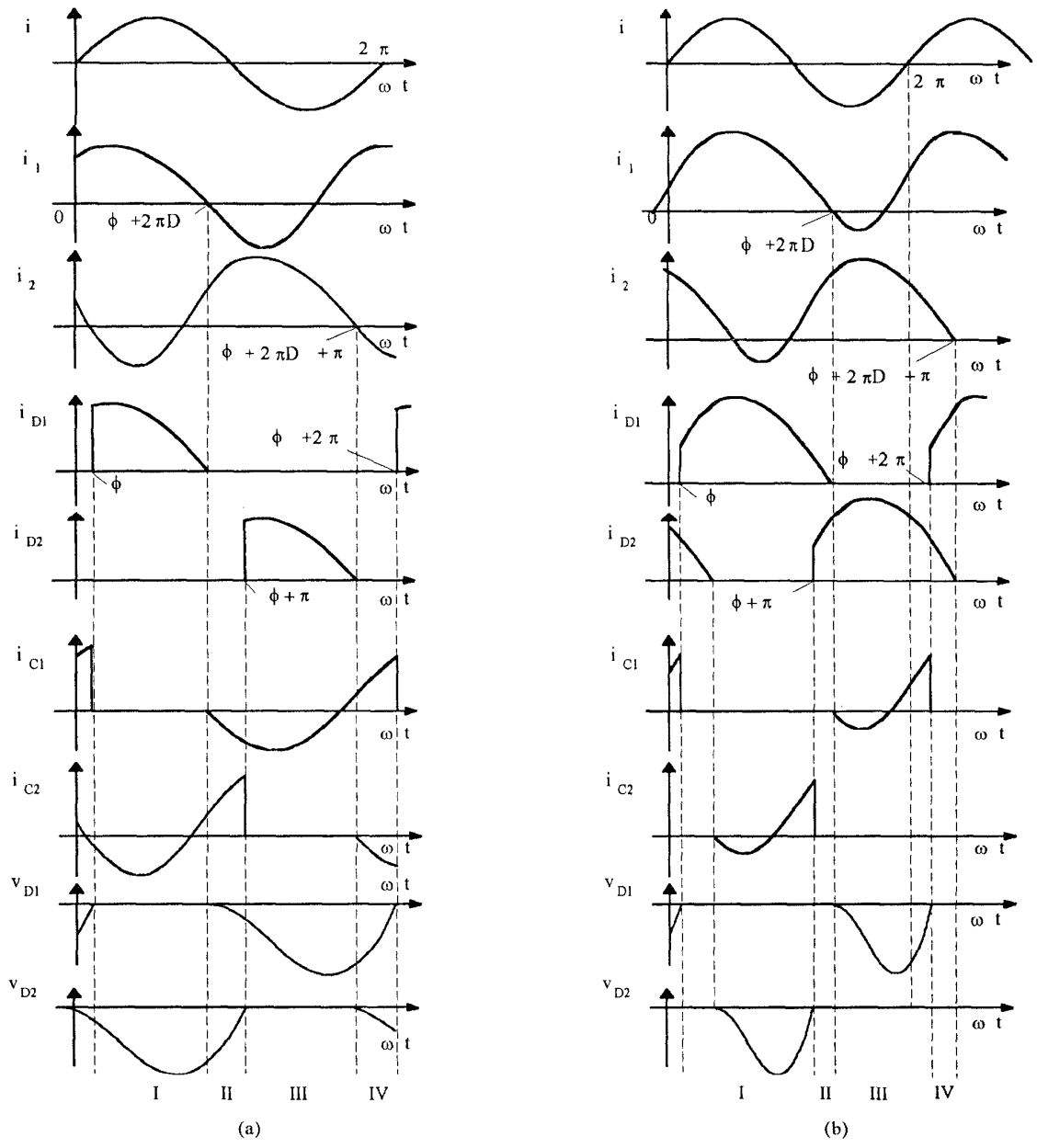

Fig. 2. Current and voltage waveforms in a class E current-driven center-tapped low *dv/dt* rectifier. a) Operation at $0 < D \leq 0.5$. b) Operation at $0.5 < D \leq 1$.

The equivalent circuits of the rectifier are linear during each interval given in Table I. Therefore, the Laplace transform can be used to analyze the rectifier circuit. Moreover, the relationship between the currents through the three transformer windings is given by

$$i(t) = \frac{1}{n}\left[i_1(t) - i_2(t)\right]. \tag{2}$$

Combinations of (1) and (2) with equations resulting from the analysis of the four equivalent circuits of the rectifiers during one switching period allows for the derivation of the current and voltage expressions. As an examples, the equations of currents i_1 and i_2 and voltages $v_{D1} = v_{C1}$ and $v_{D2} = v_{C2}$ for each topological mode of a rectifier operated at $0 < D \leq 0.5$ are given below.

A. First Topological Mode: $\phi < \omega t \leq \phi + 2\pi D$

$$i_1 = nI_m \sin \omega t + \left\{ \cos\phi \left[\omega^2 \sin(\omega t - \phi) - \frac{\omega\omega_o}{\sqrt{2}} \sin\left[\frac{\omega_o}{\sqrt{2}} \left(t - \frac{\phi}{\omega} \right) \right] \right] + \sin\phi \left[\omega^2 \cos(\omega t - \phi) - \frac{\omega_o^2}{2} \cos\left[\frac{\omega_o}{\sqrt{2}} \left(t - \frac{\phi}{\omega} \right) \right] \right] \right\} + \frac{[i_1(\phi) + i_2(\phi)]}{2} \cos\left[\frac{\omega_o}{\sqrt{2}} \left(t - \frac{\phi}{\omega} \right) \right] - \frac{[2Vo + v_{C1}(\phi) + v_{C2}(\phi)]}{\sqrt{2}\omega_o L} \sin\left[\frac{\omega_o}{\sqrt{2}} \left(t - \frac{\phi}{\omega} \right) \right] \quad (3)$$

$$i_2 = \frac{nI_m}{(\omega_o^2 - 2\omega^2)} \times \left\{ \cos\phi \left[\omega^2 \sin(\omega t - \phi) - \frac{\omega\omega_o}{\sqrt{2}} \sin\left[\frac{\omega_o}{\sqrt{2}} \left(t - \frac{\phi}{\omega} \right) \right] \right] + \sin\phi \left[\omega^2 \cos(\omega t - \phi) - \frac{\omega_o^2}{2} \cos\left[\frac{\omega_o}{\sqrt{2}} \left(t - \frac{\phi}{\omega} \right) \right] \right] \right\} + \frac{i_1(\phi) + i_2(\phi)}{2} \cos\left[\frac{\omega_o}{\sqrt{2}} \left(t - \frac{\phi}{\omega} \right) \right] - \frac{2Vo + v_{C_1}(\phi) + v_{C_2}(\phi)}{\sqrt{2}\omega_o L} \sin\left[\frac{\omega_o}{\sqrt{2}} \left(t - \frac{\phi}{\omega} \right) \right] \quad (4)$$

$$v_{C1} = 0 \quad (5)$$

$$v_{C2} = \frac{nI_m}{(\omega_o^2 - 2\omega^2)C} \times \left\{ -\omega \cos\phi \left[\cos(\omega t - \phi) - \cos\left(\frac{1}{\sqrt{2}} \left(\frac{\omega_o t}{\omega} - \phi \right) \right) \right] + \sin\phi \left[\omega \sin(\omega t - \phi) - \frac{\omega_o}{\sqrt{2}} \sin\left(\frac{1}{\sqrt{2}} \left(\frac{\omega_o t}{\omega} - \phi \right) \right) \right] \right\} + \frac{[i_1(\phi) + i_2(\phi)]}{2\omega_o C} \sin\left(\frac{1}{\sqrt{2}} \left(\frac{\omega_o t}{\omega} - \phi \right) \right) + \left[v_{C_1}(\phi) + v_{C_1}(\phi) + 2Vo \right] \left[\cos\left(\frac{1}{\sqrt{2}} \left(\frac{\omega_o t}{\omega} - \phi \right) \right) - 1 \right] + v_{C_2}(\phi) \quad (6)$$

B. Second Topological Mode: $\phi + 2\pi D \leq \omega t \leq \phi + \pi$

$$i_1 = n \frac{I_m}{2} \sin\omega t + \frac{1}{2} [i_1(\phi + 2\pi D) + i_2(\phi + 2\pi D)] \times \cos\left[\omega_o \left(t - \frac{\phi}{\omega} - \frac{2\pi D}{\omega} \right) \right] - \frac{[v_{C1}(\phi + 2\pi D) + v_{C2}(\phi + 2\pi D) + 2Vo]}{2\omega_o L} \times \sin\left[\omega_o \left(t - \frac{\phi}{\omega} - \frac{2\pi D}{\omega} \right) \right] \quad (7)$$

$$i_2 = -n \frac{I_m}{2} \sin\omega t + \frac{1}{2} [i_1(\phi + 2\pi D) + i_2(\phi + 2\pi D)] \times \cos\left[\omega_o \left(t - \frac{\phi}{\omega} - \frac{2\pi D}{\omega} \right) \right] - \frac{[v_{C1}(\phi + 2\pi D) + v_{C2}(\phi + 2\pi D) + 2Vo]}{2\omega_o L} \times \sin\left[\omega_o \left(t - \frac{\phi}{\omega} - \frac{2\pi D}{\omega} \right) \right] \quad (8)$$

$$v_{C1} = nI_m \frac{\cos\omega t - 1}{2\omega C} + \frac{i_1(\phi + 2\pi D) + i_2(\phi + 2\pi D)}{2} \sin\left[\omega_o \left(t - \frac{\phi}{\omega} - \frac{2\pi D}{\omega} \right) \right] + \frac{v_{C1_1}(\phi + 2\pi D)}{2} \cos\left[\omega_o \left(t - \frac{\phi}{\omega} - \frac{2\pi D}{\omega} \right) \right] + \frac{v_{C1}(\phi + 2\pi D) + 2Vo}{2} \cos\left[\omega_o \left(t - \frac{\phi}{\omega} - \frac{2\pi D}{\omega} \right) \right] - \frac{v_{C1_1}(\phi + 2\pi D) + v_{C2}(\phi + 2\pi D) + 2Vo}{2} + v_{C1}(\phi + 2\pi D) \quad (9)$$

C. Third Topological Mode: $\phi + \pi < \omega t \le \phi + \pi + 2\pi D$

$$i_1 = -\frac{nI_m}{\omega_o^2 - 2\omega^2}$$
$$\text{x}\Bigg\{ \cos(\phi+\pi)\omega^2 \sin(\omega t - \phi - \pi)$$
$$- \cos(\phi+\pi)\frac{\omega\omega_o}{\sqrt{2}}\sin\left[\frac{\omega_o}{\sqrt{2}}\left(t - \frac{\phi}{\omega} - \frac{\pi}{\omega}\right)\right] +$$
$$+\sin(\phi+\pi)\left[\omega^2\cos(\omega t - \phi - \pi)\right.$$
$$\left.\left. + \frac{\omega_o^2}{2}\cos\left[\frac{\omega_o}{\sqrt{2}}\left(t - \frac{\phi}{\omega} - \frac{\pi}{\omega}\right)\right]\right]\right\}$$
$$+ \frac{i_1(\phi+\pi) + i_2(\phi+\pi)}{2}\cos\left[\frac{\omega_o}{\sqrt{2}}\left(t - \frac{\phi}{\omega} - \frac{\pi}{\omega}\right)\right]$$
$$- \frac{2V_O + v_{C1}(\phi+\pi) + v_{C2}(\phi+\pi)}{\sqrt{2}\omega_o L}\sin\left[\frac{\omega_o}{\sqrt{2}}\left(t - \frac{\phi}{\omega} - \frac{\pi}{\omega}\right)\right] \quad (10)$$

$$i_2 = nI_m \sin\omega t$$
$$- \frac{nI_m}{\omega_o^2 - 2\omega^2}\{\cos(\phi+\pi)\omega^2\sin(\omega t - \phi - \pi)$$
$$- \cos(\phi+\pi)\frac{\omega\omega_o}{\sqrt{2}}\sin\left[\frac{\omega_o}{\sqrt{2}}\left(t - \frac{\phi}{\omega} - \frac{\pi}{\omega}\right)\right] +$$
$$+\sin(\phi+\pi)\left[\omega^2\cos(\omega t - \phi - \pi)\right.$$
$$\left.\left. - \frac{\omega_o^2}{2}\cos\left[\frac{\omega_o}{\sqrt{2}}\left(t - \frac{\phi}{\omega} - \frac{\pi}{\omega}\right)\right]\right]\right\}$$
$$+ \frac{i_1(\phi+\pi) + i_2(\phi+\pi)}{2}$$
$$\text{x}\cos\left[\frac{\omega_o}{\sqrt{2}}\left(t - \frac{\phi}{\omega} - \frac{\pi}{\omega}\right)\right]$$
$$- \frac{2V_O + v_{C1}(\phi+\pi) + v_{C2}(\phi+\pi)}{\sqrt{2}\omega_o L}$$
$$\text{x}\sin\left[\frac{\omega_o}{\sqrt{2}}\left(t - \frac{\phi}{\omega} - \frac{\pi}{\omega}\right)\right] \quad (11)$$

$$v_{C2} = 0 \quad (12)$$

$$v_{C1} = -\frac{nI_m}{C\left(\omega_o^2 - 2\omega^2\right)}$$
$$\text{x}\{-\omega\cos(\phi+\pi)\cos(\omega t - \phi - \pi)$$
$$+ \omega\cos(\phi+\pi)\cos\left[\frac{\omega_o}{\sqrt{2}}\left(t - \frac{\phi}{\omega} - \frac{\pi}{\omega}\right)\right]$$
$$+\sin(\phi+\pi)\left[\omega\sin(\omega t - \phi - \pi)\right]$$
$$\left. - \frac{\omega_o}{\sqrt{2}}\sin\left[\frac{\omega_o}{\sqrt{2}}\left(t - \frac{\phi}{\omega} - \frac{\pi}{\omega}\right)\right]\right\}$$
$$+ \frac{i_1(\phi+\pi) + i_2(\phi+\pi)}{2\omega_o C}$$
$$\text{x}\sin\left[\frac{\omega_o}{\sqrt{2}}\left(t - \frac{\phi}{\omega} - \frac{\pi}{\omega}\right)\right] +$$
$$+\left[v_{C1}(\phi+\pi) + v_{C2}(\phi+\pi) + 2Vo\right]$$
$$\text{x}\left[\cos\left[\frac{\omega_o}{\sqrt{2}}\left(t - \frac{\phi}{\omega} - \frac{\pi}{\omega}\right)\right] - 1\right] + v_{C1}(\phi+\pi) \quad (13)$$

D. Fourth Topological Mode: $\phi + \pi + 2\pi D < \omega t \le \phi + 2\pi$

$$i_1 = n\frac{I_m}{2}\sin\omega t$$
$$+ \frac{1}{2}\left[i_1(\phi + 2\pi D + \pi)\right]\cos\left[\omega_o\left(t - \frac{\phi - 2\pi D - \pi}{\omega}\right)\right]$$
$$+ \frac{1}{2}\left[i_2(\phi + 2\pi D + \pi)\right]\cos\left[\omega_o\left(t - \frac{\phi - 2\pi D - \pi}{\omega}\right)\right]$$
$$- \frac{v_{C1}(\phi + 2\pi D + \pi)}{(2\omega_o L)}\sin\left[\omega_o\left(t - \frac{\phi - 2\pi D - \pi}{\omega}\right)\right]$$
$$- \frac{v_{C2}(\phi + 2\pi D + \pi) + 2Vo}{2\omega_o L}\sin\left[\omega_o\left(t - \frac{\phi - 2\pi D - \pi}{\omega}\right)\right] \quad (14)$$

$$i_2 = -n\frac{I_m}{2}\sin(\omega t)$$
$$+ \frac{1}{2}\left[i_1(\phi + 2\pi D + \pi)\right]\cos\left[\omega_o\left(t - \frac{\phi - 2\pi D - \pi}{\omega}\right)\right]$$
$$+ \frac{1}{2}\left[i_2(\phi + 2\pi D + \pi)\right]\cos\left[\omega_o\left(t - \frac{\phi - 2\pi D - \pi}{\omega}\right)\right]$$
$$- \frac{v_{C1}(\phi + 2\pi D + \pi)}{2\omega_o L}\sin\left[\omega_o\left(t - \frac{\phi - 2\pi D - \pi}{\omega}\right)\right]$$
$$- \frac{v_{C2}(\phi + 2\pi D + \pi) + 2V_O}{2\omega_o L}\sin\left[\omega_o\left(t - \frac{\phi - 2\pi D - \pi}{\omega}\right)\right] \quad (15)$$

$$v_{C1} = -nI_m \frac{\cos\omega t - 1}{2\omega C} + \frac{i_1(\phi + 2\pi D + \pi)}{2} \sin\left[\omega_o\left(t - \frac{\phi - 2\pi D - \pi}{\omega}\right)\right] + \frac{i_2(\phi + 2\pi D + \pi)}{2} \sin\left[\omega_o\left(t - \frac{\phi - 2\pi D - \pi}{\omega}\right)\right] + \frac{v_{C1}(\phi + 2\pi D + \pi)}{2} \cos\left[\omega_o\left(t - \frac{\phi - 2\pi D - \pi}{\omega}\right)\right] + \frac{v_{C2}(\phi + 2\pi D + \pi)}{2} \cos\left[\omega_o\left(t - \frac{\phi - 2\pi D - \pi}{\omega}\right)\right] + Vo\cos\left[\omega_o\left(t - \frac{\phi - 2\pi D - \pi}{\omega}\right)\right] + v_{C1}(\phi + 2\pi D + \pi) - \frac{v_{C1}(\phi + 2\pi D + \pi) + v_{C2}(\phi + 2\pi D + \pi) + 2Vo}{2} \quad (16)$$

$$v_{C2} = nI_m \frac{\cos\omega t - 1}{2\omega C} + \frac{i_1(\phi + 2\pi D + \pi)}{2} \sin\left[\omega_o\left(t - \frac{\phi - 2\pi D - \pi}{\omega}\right)\right] + \frac{i_2(\phi + 2\pi D + \pi)}{2} \sin\left[\omega_o\left(t - \frac{\phi - 2\pi D - \pi}{\omega}\right)\right] + \frac{v_{C1}(\phi + 2\pi D + \pi)}{2}\left\{\cos\left[\omega_o\left(t - \frac{\phi - 2\pi D - \pi}{\omega}\right)\right] - 1\right\} + \frac{v_{C2}(\phi + 2\pi D + \pi)}{2}\left\{\cos\left[\omega_o\left(t - \frac{\phi - 2\pi D - \pi}{\omega}\right)\right] - 1\right\} + V_O\left\{\cos\left[\omega_o\left(t - \frac{\phi - 2\pi D - \pi}{\omega}\right)\right] - 1\right\} + v_{C2}(\phi + 2\pi D + \pi) \quad (17)$$

where $\omega_O = 1/\sqrt{LC}$.

Combination of (1) to (17) allows for the calculation of parameters such as ϕ, D, the dc output current I_O, the maximum current through each diode I_{DM}, and the maximum reverse voltage across each diode V_{DM}. Unfortunately, the expressions of these quantities cannot be derived in a closed form. For this reason, a computer program has been developed to calculate these parameters.

Fig. 3 shows a plot of D as a function of load resistance R_L for f_o = 4.9 MHz (resulting from L = 15 nH and C_P = 70 nF) and a constant output voltage normalized with respect to the transformer turns ratio V_O/n = 0.275 (it has been assumed that V_O = 3.3 V and n = 12). The diode duty cycle decreases as the output current decreases. Therefore, the current through the diodes becomes more impulsive at light loads. Moreover, a small variation of D is needed to regulate the output voltage over a wide load range, e.g., duty cycle D decreases from 0.6 to 0.45 for a load resistance increasing from 0.14 Ω to 1.4 Ω.

Figs. 4 depicts a plot of the maximum current through the transformer primary winding I_m of R_L at f_O = 4.9 MHz and V_O/n = 0.27. Current I_m increases from 0.5 A to 5 A as the dc output current I_O increases from 2.3 A to 23 A. Therefore, both the dc output current and the primary current range in the same relative interval, e.g., 1 to 10 or 10% to 100%.

Both I_m and D depend on ω_O and V_O/n while the diode maximum current and voltage are independ of these parameters.

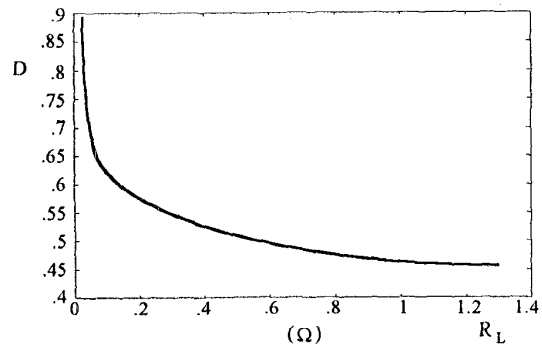

Fig. 3. Duty cycle D versus load resistance R_L.

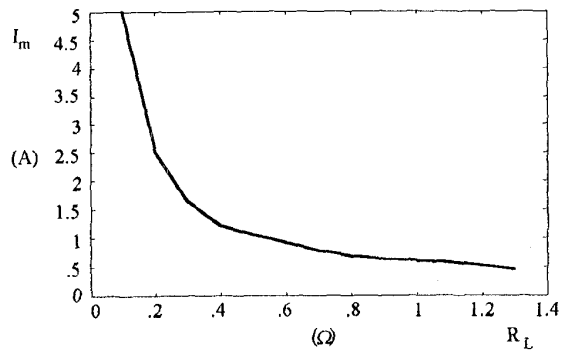

Fig. 4. Amplitude of primary current I_m as a function of R_L at f_o = 4.9 MHz and V_O/n = 0.27.

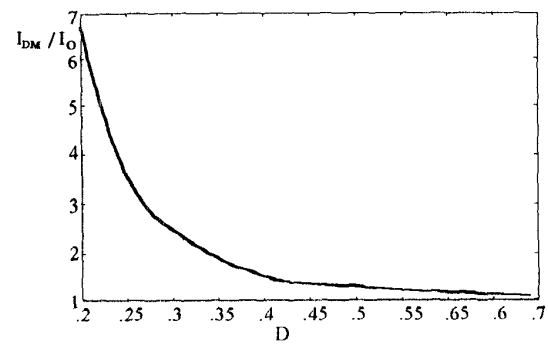

Fig. 5. Normalized maximum current I_{DM}/I_O as a function of duty cycle D.

Fig. 5 shows I_{DM} normalized with respect to I_O as a function of D. The maximum normalized current through the diodes decreases from 1.5 to 1.1 as D increases from 0.4 to 0.6. Since D is in the range of 0.45–0.6 for a load resistance decreasing from 1.4 to 0.14, the maximum current through the diodes increases from 3.45 to 25 A for a dc output current

ranging from 2.3 to 23 A. This shows that the current through the diodes does not significantly exceeds the dc output current when the rectifier is operated at full load.

A plot of V_{DM} normalized with respect to V_O as a function of D is shown in Fig. 6. The maximum normalized reverse voltage across the rectifier diodes increases from 3.5 to 4.3 for D increasing from 0.45 to 0.6. For a rectifier operated at an output voltage V_O = 3.3 V and a load resistance in the range to 0.14 to 14 W, the maximum voltage across the diodes increases from 11.5 V at full load to 14.2 V at light load. Because of the low values of V_{DM}, Schottky diodes can be used in the rectifier circuits. This allows for a high-frequency operation of the rectifier.

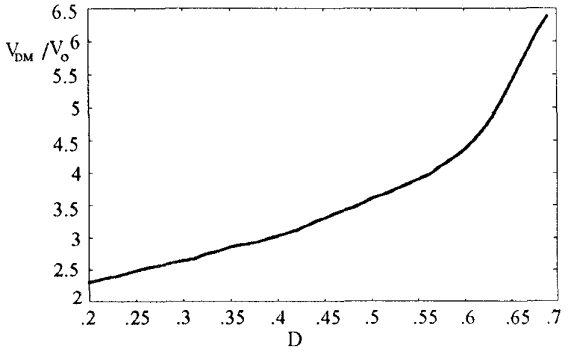

Fig. 5. Normalized maximum diode reverse voltage V_{DM}/V_O as a function of duty cycle D.

IV. Design Example And Experimental Results

A a full-range off-line power supply based on class DE dc-dc converter with a class D series resonant inverter and a class E current-driven center-tapped low *dv/dt* rectifier was built to operate at an input dc voltage V_I = 120 to 370 V_{dc}, a regulated output voltage V_O = 3.3 V, an output power P_O = 60 W, and a nominal operating frequency f = 500 kHz. The maximum output current of the converter was I_{OM} = 18 A, which corresponds to a minimum load resistance R_{Lmin} = 0.18 Ω. The converter circuit was designed for the minimum input voltage and maximum load operation. The dc-to-dc voltage transfer function of the entire converter was $M_{max} = V_O / V_{Imin} = 3.3 / 120 = 0.0275$. A class D series resonant inverter operated at a voltage transfer function M_{Imax} = 0.383 was used as a sinusoidal current source. Therefore, the rectifier voltage transfer function was $M_R = M_{max} / M_{Imax} = 0.0275 / 0.383 = 0.072$. As a result, the amplitude of the fundamental component of the primary winding voltage in phase with the primary current was calculated as $V_{Rm} = \sqrt{2}\ V_O / M_R = 64.8$ V and the transformer turns ratio was n = 12.

The center-tapped transformer was built on a EFD30 Siemens N49 ferrite core. The primary was wound with 24 turns of AWG22 solid copper wire and the two secondary windings with 2 turns of copper strips 15 *x* 0.15 mm each. The measured transformer magnetizing inductance was L_m = 1.23 mH, the equivalent series resistance (ESR) of the three windings seen across the terminals of the primary winding was R_S = 0.63 Ω, f = 500 kHz and each secondary leakage inductance was L = 18 nH. Two International Rectifier 32CTQ30 Schottky diodes were used in the rectifier. An external capacitance C_P = 66 nF was connected in parallel with each diode. Two electrolytic Oscon 100 μF / 20 V capacitors connected in parallel were used as filter capacitors. Fig. 6 shows experimental voltage and current waveforms of the transformer primary winding at V_I = 110 V and f = 465 kHz. Fig. 7 shows the experimental waveforms of the voltages across diodes D_1 and D_2. The measured efficiency of the ac-dc converter including the front-end full-bridge transfromerless rectifier is plotted in Fig. 8 as a function of I_O. The measured efficiency at the full load operation at a low line voltage V_{Irms} = 120 V was η = 81 % and was 1.5% higher than the efficiency measured at V_{Irms} = 220 V over the entire load range.

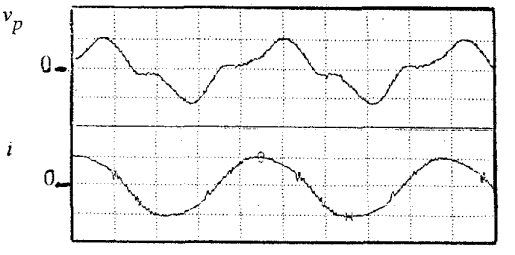

Fig. 6. Waveforms of voltage and current for the primary winding for the transformer at an operating frequency f = 465 kHz, ac input voltage V_{Irms} = 110 V, output voltage V_O = 3.3 V, and R_L = 0.18 Ω. Vertical: 100 V/div. for v_p and 2 A/div. for i; horizontal 500 ns/div.

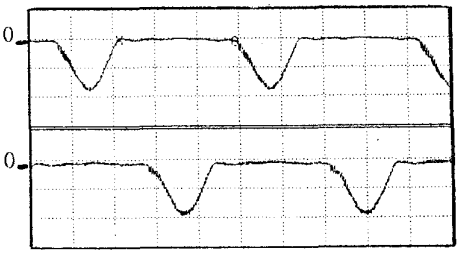

Fig. 7. Waveforms of the reverse voltage on each diode at an operating frequency f = 465 kHz, ac input voltage V_{Irms} = 110 V, output voltage V_O = 3.3 V, and R_L = 0.18 Ω. Vertical: 10 V/div.; horizontal 500 ns/div.

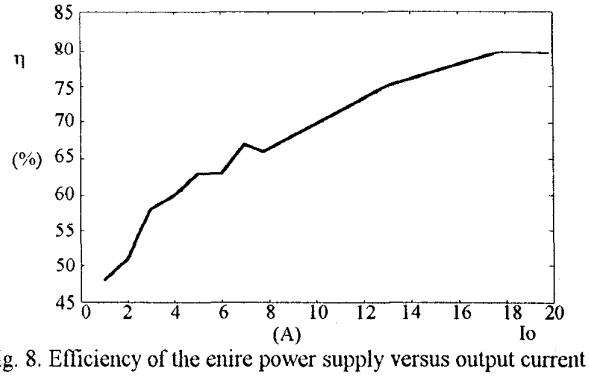

Fig. 8. Efficiency of the enire power supply versus output current at an ac input voltage V_{Irms} = 220 V and V_O = 3.3 V.

V. Conclusions

The analysis, design procedure, and experimental verification of a class E current-driven center-tapped low *dv/dt* rectifier have been presented. The leakage inductances of the transformer have been taken into account. In the class E rectifier, each diode turns on and of at zero voltage with a limited *dv/dt* at the turn-off and *dv/dt* = 0 at the turn-on. Moreover, *di/dt* is limited at the diode turn-off and a soft-reverse recovery of diodes is achieved. The class E current-driven center-tapped low *dv/dt* rectifier has been used to build a 60 W power supply operated at a line voltage varying from 85 to 260 V_{rms} and a regulated output voltage V_O = 3.3 V. A maximum efficiency η = 80 % has been achieved for the whole power supply at the maximum output current I_O = 18 A and input ac voltage V_{Irms} = 220 V.

Since zero-voltage turn-on of the switches is achieved, the rectifier efficiency can be increased if diodes are replaced by low on-resistance power MOSFETs. Theoretical analysis and experimental verifications of the class E current-driven center-tapped synchronous rectifier are recommended for future work.

References

[1] M. K. Kazimierczuk, "Class E dv_D/dt rectifier," *Proc. Inst. Elec. Eng., Part B, Electric Power Appl.*, vol. 136, pp. 257-262, Nov. 1989.

[2] M. K. Kazimierczuk, and X.T. Bui, "A family of class E resonant dc-dc power converters," *Proc. 16th Intern. PCI '88 Conf. (SATECH '88)*, Dearborn, MI, pp.383-394, Oct. 3-6, 1988.

[3] J. Jozwik and M.K. Kazimierczuk, "Analysis and design of Class E^2 dc-dc converter," *IEEE Trans. Ind. Electron.*, vol IE-37, pp.173-183, April 1990.

[4] A. Reatti, M. K. Kazimierczuk, "Efficiency of the class E half-wave low dv_D/dt rectifier," *Proccedings of ISCAS'93*, Chicago, USA, Vol. 4, pp. 2331-2334, May 3-6, 1993.

[5] A. Reatti, M. K. Kazimierczuk, "Comparison of the efficiencies of class D and class E rectifiers," *Proceeding of 36th Midwest Symposium on Circuits and Systems*, Detroit, USA, Vol. 2, pp. 872-874, August 16-18, 1993.

[6] M. Bartoli, A. Reatti, M. K. Kazimierczuk, "Efficiency of a class E dc-dc converter with a center tapped rectifier at any loaded quality factor," *Proceedings of 37th Midwest Symposium on Circuits Systems*, Lafayette, LA, August 3-5, 1994, pp. 678-681.

[7] A. Reatti, M. K. Kazimierczuk, and R. Redl, "Class E full-wave low dv/dt rectifier," *IEEE. Transactions on Circuits and Systems*, Part I, 40, 73-85, February 1993.

[8] Kazimierczuk, M. K. and K. Puczko, "Power-output capability of class E amplifier at any loaded Q and switch duty cycle," *IEEE Trans. Circuits Syst.*, vol CAS-36, pp. 1142-1144, August 1989.

[9] K. Schmidtner, "A new high frequency resonant converter topology," *Proc. High Freq. Power Conversion Conf.*, pp.390-403, San Diego, CA, May 1988.

[10] S.L. Smith and S. Robinson, "An off-line, one MHz 350-Watt parallel resonant converter (PRC) utilizing an RF transformer," *High Frequency Power Conversion Conference*, San Diego, CA, pp. 446-466, May 1988.

[11] R. Myers and R.D. Peck, "200-KHz Power FET Technology in New Modular Power Supplies," *Hewlett-Packard Journal*, pp. 3-10, August 1981.

[12] V. Vorpérian and S. Cuk, "A complete dc analysis of the series resonant converter," in *IEEE Power Eletron. Specialists Conf. Rec.*, Cambridge, MA, pp. 85-100, June 14-17, 1982.

[13] R. L. Steigerwald, "High-frequency resonant transistor dc-dc converter," *IEEE Trans. Power Electron.*, pp. 181-191, May 1984.

[14] R. L. Steigerwald, "A comparison of half-bridge resonant converter topologies," *IEEE Trans. Power Electron.*, vol. PE-3, pp. 174-182, April 1988.

[15] R. J. King and T. A. Stuart, "A normalized model for the half-bridge series resonant converter," *IEEE Trans. Aerospace Electron. Syst.*, vol. AES-17, pp. 190-198, Mar. 1981.

[16] M. K. Kazimierczuk, and S. Wang, "Frequency domain analysis of series converter for continuous conduction mode," *IEEE Trans. Power Electron.*, Vol. 7, No. 2, pp. 270-279, Apr. 1992.

[17] M. K. Kazimierczuk, N. Thirunarayan, and S. Wang, "Analysis of series parallel resonant converters," *IEEE Trans. Aerospace Electron. Syst.*, Vol. 29, No. 1, pp. 88-99, January 1993.

[18] M. K. Kazimierczuk, and W. Szaraniec, "Class D zero-voltage-switching inverter with only one shunt capacitor," *Proc. Inst. Elect. Eng., Pt. B, Elec. Power Appl.*, vol. 139, Nov. 1992.

[19] M. K. Kazimierczuk, and W. Szaraniec, "Electronic ballast for fluorescent lamps," *IEEE Trans. Power Electron.*, Vol. PE-8, pp. 386-395, Oct. 1993.

[20] M. K. Kazimierczuk, W. Szaraniec, and S. Wang, "Analysis and design of parallel resonant converter at high Q," *IEEE Trans. Aerospace Electron. Syst.*, Vol. 28, No. 1, pp. 35-50, January 1992.

[21] M. K. Kazimierczuk and D. Czarcowski, "Resonant power converters," New York: John Wiley & Sons, 1995.